Proceedings of the
Annual Stability Conference
Structural Stability Research Council
Atlanta, Georgia, April 21-24, 2026

Fire test of a 10-story cold-formed steel building after earthquake: numerical models for thermal and mechanical analysis

Yu Niu[1], Joshua Dillard[2], Richard Emberley[3], Tara Hutchinson[4], Brian Meacham[5], Thomas Gernay[6]

Abstract

This paper describes the numerical modeling of fire tests conducted in July 2025 on a 10-story cold-formed steel (CFS) building at UC San Diego. The full-scale CFS building underwent seismic tests followed by fire tests, providing unique experimental data for benchmarking computational models. Numerical models were used before the tests to gain understanding in the anticipated response and were refined after the tests to further analyze the observed behavior. The FE models integrate 2D and 3D thermal analysis with 3D thermal-mechanical analysis. The thermal analyses evaluate temperature rise in the steel members accounting for protection from the gypsum, with 3D thermal models used to assess the effect of non-uniform thermal exposure along the walls. The computed transient steel temperatures are then used as input for the shell analysis of the loaded structure to assess stability throughout the fire. Comparison between model predictions and test observations shows good agreement in steel temperatures, with limited effect of the gradient between the bottom and top of the room. The calibrated models are then used to evaluate the effect of fasteners and loading on failure temperature, confirming that the vertical load-bearing system in the tested structure had significant reserve in resistance during the fire test. This research leverages a unique full-scale post-seismic fire testing program with advanced computational models to enhance understanding of the fire performance of thin-walled CFS buildings.

1. Introduction

Post-seismic fires pose a threat to public safety because an earthquake can both ignite fires and degrade the community's firefighting capacity (Scawthorn *et al.*, 2005; Lee *et al.*, 2008). Studying post-seismic fire resilience is also important to understand the impact of moderate seismic damage on fire performance and the repairs needed after an earthquake. In cold-formed steel (CFS) construction, the fire resistance of CFS members relies on protective systems such as gypsum sheathing and their connections, which may be damaged by a preceding earthquake (Hutchinson *et al.*, 2021). As CFS systems are increasingly proposed for use as load-bearing systems in midrise buildings (Torabian *et al.*, 2016), advancing understanding of the post-earthquake fire performance of CFS building components is important for safety and resilience.

[1] PhD Student, Johns Hopkins University, yniu11@jhu.edu
[2] Master's Student, Johns Hopkins University, jdillar6@jh.edu
[3] Associate Professor, California Polytechnic State University, remberle@calpoly.edu
[4] Professor & Jan Talbot Endowed Chair, University of California San Diego, tahutchinson@ucsd.edu
[5] PhD, Meacham Associates, brian.meacham@meachamassociates.com
[6] Associate Professor, Johns Hopkins University, tgernay@jhu.edu

In 2016, a full-scale, six-story CFS building fire-following-earthquake test showed that the earthquake caused cracking of gypsum boards and detachment of fasteners in some walls, and that the subsequent fire led to degradation of sheathing, thermal bowing, and partial ceiling detachment, amongst other damage (Hutchinson *et al.*, 2021). In 2025, as part of the CFS-NHERI project to investigate a beyond-code CFS building, two new fire-following-earthquake tests were conducted on a 31.6 m tall CFS-framed building on the shake table at UC San Diego. The fire tests were designed to last longer than the 2016 tests and to include instrumentation to measure temperature on the CFS framing members. Prior to the CFS-10 tests, numerical models predicted how different levels of earthquake-induced damage would affect the fire response of key building structural members, to inform the test setup (Niu *et al.*, 2025). These studies also built on recent investigations into the fire behavior of CFS members, such as experiments on CFS material properties at elevated temperatures (Kankanamge and Mahendran, 2011; Yan *et al.*, 2020) which led to provisions in design specifications (*ANSI/SDI AISI S100*, 2024), and data on the thermal properties of gypsum sheathing (Cooper, 1997), the temperature-dependent degradation of gypsum-to-steel fastener stiffness (Abreu *et al.*, 2021), and the fire resistance of CFS members under steady-state uniform heating (Bandula Heva and Mahendran, 2013), steady-state nonuniform heating (Xie and Gernay, 2025), and transient fire exposures (Feng *et al.*, 2003; Gunalan, 2011). Numerical studies have also examined the fire resistance of CFS members under steady-state uniform (Gunalan *et al.*, 2014) and nonuniform heating (Ali, 2021) and transient fire scenarios (Ariyanayagam and Mahendran, 2014).

To advance multi-hazard resilience of CFS buildings and support code advancement, there remains a need for data and validated models on the post-earthquake fire response of the structure. In a post-seismic fire scenario, the earthquake can damage the nonstructural components that protect and restrain CFS members, such as the gypsum sheathing and fasteners (Hutchinson *et al.*, 2017; Chen *et al.*, 2020). Yet, there is still a lack of understanding of how earthquake-induced damage to gypsum boards and fasteners affects the fire resistance of CFS members. Although predictions (Niu *et al.*, 2025) were made through modeling prior to the CFS10 test, the test had not been completed at that time, so the model could not be validated by comparison with experimental results. In addition, for safety reasons the CFS10 fire tests were designed to avoid structural failure. Modeling can complement these tests to examine the response to failure.

Therefore, the objective of this paper is threefold: (i) to validate the 2D and 3D thermal FE models by comparing them with experimental results; (ii) to examine the sensitivity of the fire response of CFS studs to earthquake-induced damage to gypsum boards and fasteners; and (iii) to model the structural fire response of the tested members under increasing applied loads to assess the safety margin. Thermal analysis models of wall assemblies are validated against the CFS10 test data. The computed nonuniform temperature histories are used in 3D shell structural models, which integrate temperature-dependent steel stress-strain (ANSI/SDI AISI S100, 2024), a temperature-dependent fastener stiffness model (Abreu *et al.*, 2021), and initial geometric imperfections based on elastic buckling analysis (Adany, 2006; Li and Schafer, 2010). Thermal-structural models in SAFIR (Franssen and Gernay, 2017) are used to examine the effect of different level of damage on the CFS members fire behavior. Simulations are run under various applied loads to assess the safety margin of the studs in the CFS-10 tests.

2. CFS10 fire tests

The test specimen was a fully finished, 10-story CFS building assembled on the UC San Diego Large High-Performance Outdoor Shake Table (Figure 1a). Its footprint was 11.6 m × 6.9 m, with an overall height of 30.5 m. Conceptually, the specimen represented a "slice" taken from a larger archetype building with a 35.3 m × 14.6 m floor plan, designed for residential use (e.g., apartment or dormitory) organized around a central corridor (Torabian *et al.*, 2016). The building used a light-frame CFS stud wall system with ledger-framed, joist-supported floor framing; both gravity load support and lateral force resistance were provided by CFS-framed assemblies. Each story was divided into two compartments (Figure 1b). The west compartment had a 9-story resilient stair system. The east compartment, which was the fire test compartment, had internal dimensions of 2.6 m (height) by 4.3 m (depth) by 6.6 m (length). The north facade of the east compartment had a window of 1.22 m by 1.42 m, corresponding to an opening factor of 0.017 $m^{1/2}$. It had a multilayer exterior insulated finish system (EIFS). All walls were lined on both sides with one 15.9 mm layer of Type X fire-rated gypsum board fastened to lipped channels and tracks. In addition, a finished suspended ceiling with one layer of Type X board was used in the east compartment.

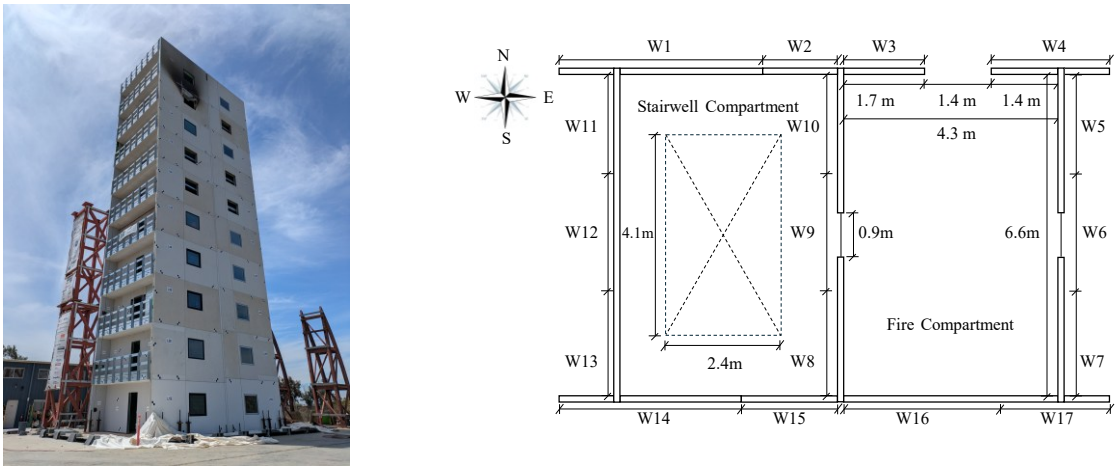

(a) (b)

Figure 1: (a) Picture of the 10-story CFS building on the UC San Diego shake table after the fire test at L9. (b) Floor plan of the building with interior dimensions of the fire compartment.

Prior to the fire tests, 18 earthquake tests were conducted. The observed damage included gypsum board cracking and fastener rotation, pull-out, and/or penetration. Two post-seismic compartment fire tests were then performed. The first test was conducted on Level 9 with a wood crib mass of 533 kg. Assuming a wood calorific value of 17.5 MJ/kg, the resulting fire load density was 334 MJ/m². The second test was conducted on Level 6 with a wood crib mass of 625 kg, corresponding to a fire load density of 391 MJ/m². The compartment had doors that were closed during the fire test and one window (1.22 m by 1.42 m) that was open from the beginning of the test. During both tests, external flaming was observed through the window during the fully developed phase. The gypsum board finish sheathing on the compartment walls and ceiling experienced severe damage, and by the end of the tests, large portions of the gypsum board had fallen off. However, most of the detachment occurred late in the fire, based on the steel temperature data.

During the fire tests, the temperatures in the compartment and in the CFS-framed assemblies were measured with Type K thermocouples. Thermocouples were applied on the CFS wall studs at

different height and width (as shown in Figure 2), as well as across the section of the wall (i.e., on the two flanges of the studs). Along the height, thermocouples were installed at 0.84 m, 1.68 m, and 2.52 m above the floor, to record temperatures at the bottom, middle, and top, respectively. Through the wall thickness, thermocouples on the exterior surface of the gypsum board were used to measure the compartment gas temperature, while thermocouples on the interior side of the gypsum board were used to measure temperatures at the hot flange (fire-exposed side) and cold flange (unexposed side) of the wall studs.

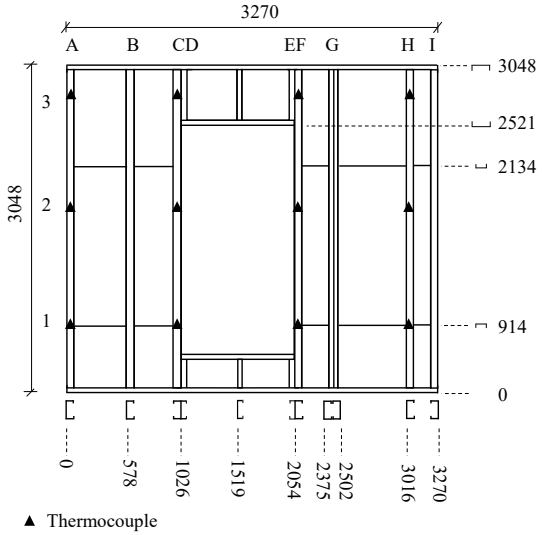

Figure 2: Thermocouple layout on wall W16

3. Thermal behavior of the CFS structure in fire

3.1. 2D Heat transfer model

Prior to the fire tests, thermal analysis models for the CFS wall assemblies (Niu *et al.*, 2025) were developed using the nonlinear FE software SAFIR. Temperature-dependent thermal properties were considered for gypsum based on Cooper (Cooper, 1997) and for steel based on EN 1993-1-2 (EN 1993-1-2, 2005). The gypsum density at ambient temperature was assumed as 648 kg/m³. Following Eurocode recommendations, the convection coefficients on the hot and cold surfaces were set to 35 W/m²·K and 4 W/m²·K, respectively, and the surface emissivity was taken as 0.7. Convection and radiation in the cavity were considered. These prior models used the predicted fire curve as input boundary conditions. After the tests, the models were run again using the measured average compartment temperature-time history as the thermal boundary condition. The results presented herein are for the gravity stud with the highest axial demand in the shear wall of the tested compartments, which was a 600S162 CFS section. The thickness and steel grade varied by story: 600S162-54(50) was used on Level 6, and 600S162-43(33) was used on Level 9. Figure 3b shows the nonuniform temperature distribution resulting from one-sided fire exposure of the wall.

3.2. 3D Heat transfer model

Building upon the 2D model, a 3D heat-transfer model was also developed in SAFIR to test the effects of the variable thermal exposure along the wall height. Indeed, recorded temperatures in the compartment showed some spatial variability in elevation. The 3D model used eight-node solid conductive finite elements to mesh the gypsum sheathing and CFS members. Radiation and

convection were considered at the surface of the exposed gypsum layer, as well as in the cavity. In the 3D model, three zones were defined corresponding to the bottom third, middle third, and top third of the wall. The measured compartment temperature averaged over each zone in the test was applied as the thermal boundary condition to the surface of the exposed gypsum at the corresponding zone. The thermal properties for the steel and gypsum were the same as in the 2D model. Figure 4 shows the model geometry with the different temperature zones.

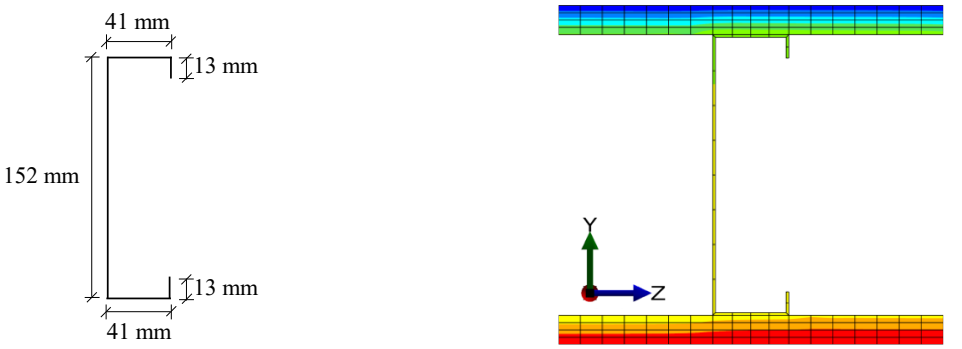

(a) 600S162 wall stud section (b) Thermal FE model of the CFS stud

Figure 3: 2D thermal analysis of a CFS channel wall section from the CFS-10 fire test

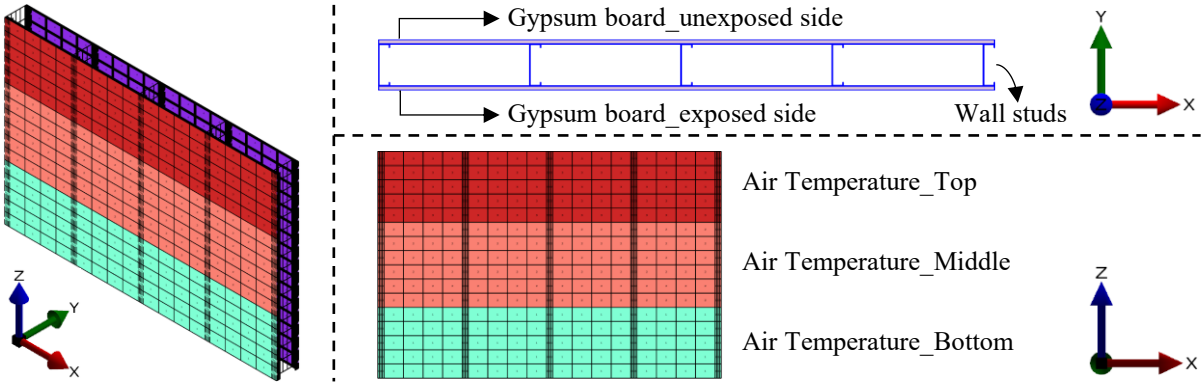

Figure 4: 3D thermal analysis of a CFS-framed wall used in the 10-story building

3.3. Comparison of test and model results for temperatures in the wall studs

Figure 5 and Figure 6 compare the measured and predicted temperatures of the hot and cold flanges of the wall studs, respectively. Data from multiple thermocouples are plotted as an envelope, and the black solid line denotes the test mean. The FE predictions fall within the measured envelope but are slightly higher than the mean values. Nevertheless, given the significant uncertainties on the behavior of the gypsum sheathing and the seismic damage, the model adequately captures the temperature evolution in the protected cold-formed steel members during the fire, enabling to evaluate the structural fire response of the members (Niu *et al.*, 2025).

The results show that the 15.9 mm Type X gypsum board provided effective thermal insulation during the fire. The peak compartment temperature exceeded the peak temperatures of the protected wall-stud hot and cold flanges by approximately 600 °C and 700 °C, respectively. In addition, the maximum temperature difference between the protected hot and cold flanges was approximately 100 °C, indicating a nonuniform thermal distribution across the stud cross-section. The limited temperature increase in the wall studs and agreement between the test data and the

model results obtained with a non-damaged gypsum board, suggest that the gypsum sheathing maintained integrity throughout most of the fire test, despite the prior 18 seismic tests.

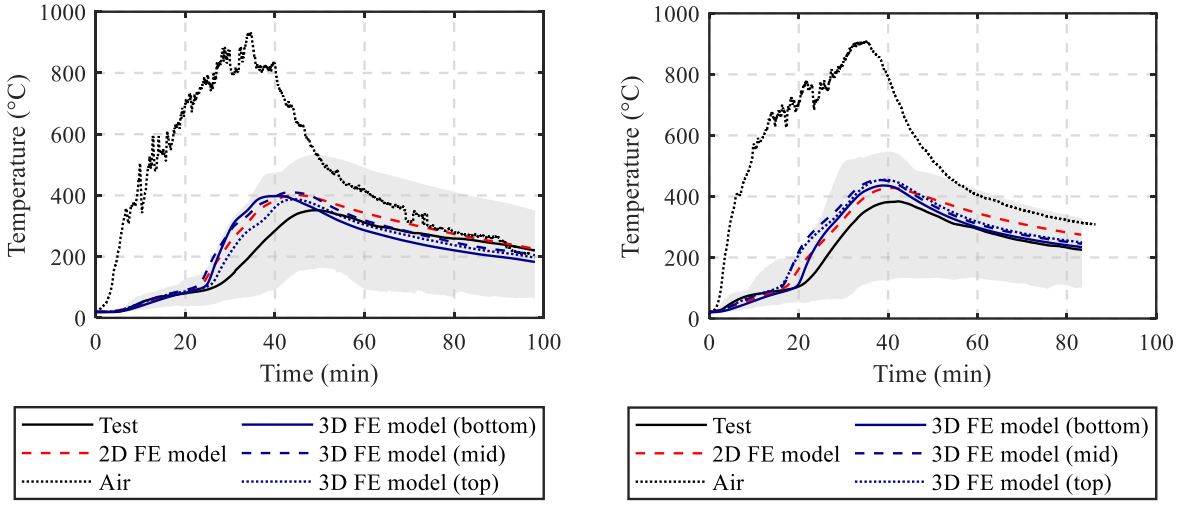

(a) L6 Test (b) L9 Test

Figure 5: Evolution of the temperature in the CFS wall studs (hot flange)

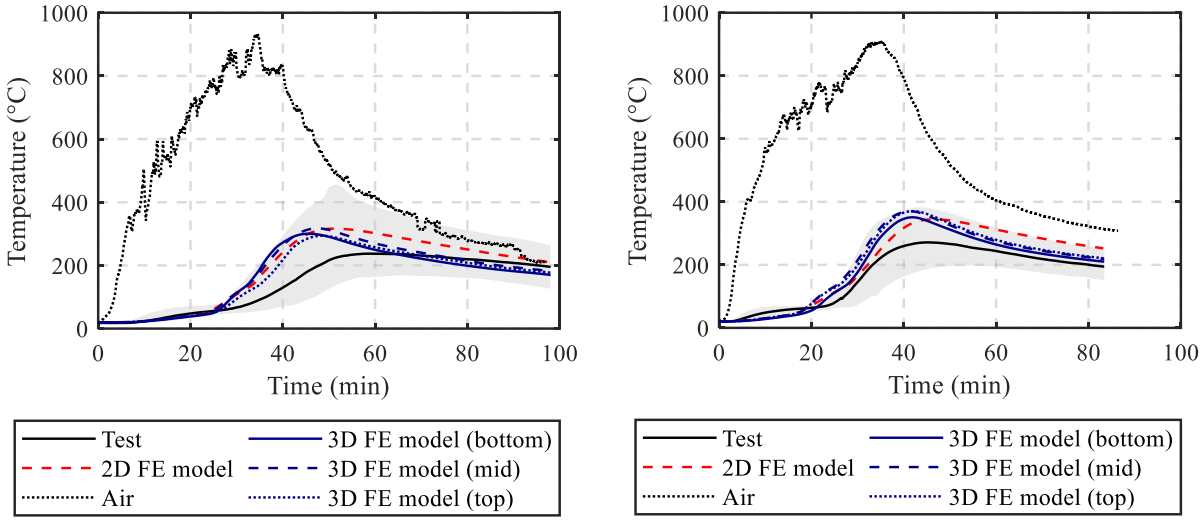

(a) L6 Test (b) L9 Test

Figure 6: Evolution of the temperature in the CFS wall studs (cold flange)

In comparing the 3D model with three different thermal boundary conditions over the height with the 2D model and experimental results, a few interesting observations can be made. First, the 3D model also aligns with the measured envelope data, which supports its validation. Second, the 3D model shows that the measured non-uniform compartment temperature along the height of the walls only results in minor variation in steel temperature along the length of the stud. This is consistent with the test results as the thermocouples placed at varying heights along the steel studs have relatively uniform temperature curves with minimal differences. Third, the 2D and 3D model exhibit similar results for both the hot and cold flanges; this supports the use of 2D heat transfer models for analyzing the wall assemblies in these tests.

4. Stability of the CFS structure in fire

4.1. FE model

The shear wall stud with the highest axial demand on Level 6 of the CFS10 building was selected for this study. The member was a 600S162-54(50) section (Figure 3a) with a length of 3048 mm. Figure 7 shows the FE model of a wall stud developed in SAFIR using nonlinear four-node quadrilateral shell elements. Each node has three translational and three rotational degrees of freedom. Initial geometric imperfections, which can strongly affect the predicted failure mode and strength of CFS members (Schafer, 2008), were defined based on buckling mode shapes. The half-wavelengths and normalized mode shapes were obtained from linear elastic buckling analysis software CUFSM. Three modes were considered: local buckling, distortional buckling, and global buckling, with corresponding imperfection amplitudes of 0.47t, 1.03t, and L/2242, respectively (Zeinoddini and Schafer, 2012), where t is the thickness and L is the member length. The steel elastic modulus and yield strength were 203 GPa and 345 MPa, respectively. The stress-strain relationship was represented using a nonlinear isotropic elastoplastic model with a softening branch and temperature-dependent mechanical properties consistent with the fire design provisions in ANSI/SDI AISI S100-24 (ANSI/SDI AISI S100, 2024). The mesh size was 6 mm × 20 mm for the lip, 10 mm × 20 mm for the flange, and 20 mm × 20 mm for the web. Pinned-pinned boundary conditions were used by restraining the X- and Z-direction translational degrees of freedom at both end cross-sections and restraining the Y-direction translational degree of freedom at the mid-height cross-section. A compressive axial load was applied using nodal loads at both ends, distributed to produce a uniform axial compressive stress over the cross-section. Load includes 1.2 times the dead load plus 0.5 times the live load in accordance with ASCE 7 (ASCE/SEI 7-22, 2022) for fire design. From a building model, the maximum load among the shear wall studs on Levels 6 was 4344 N, which was adopted in the model. The model included fasteners connecting the gypsum board to the wall stud, modeled as small fiber-based beam elements with temperature-dependent properties. The fastener stiffness was assumed to degrade with increasing temperature following the reduction model proposed in (Abreu *et al.*, 2021).

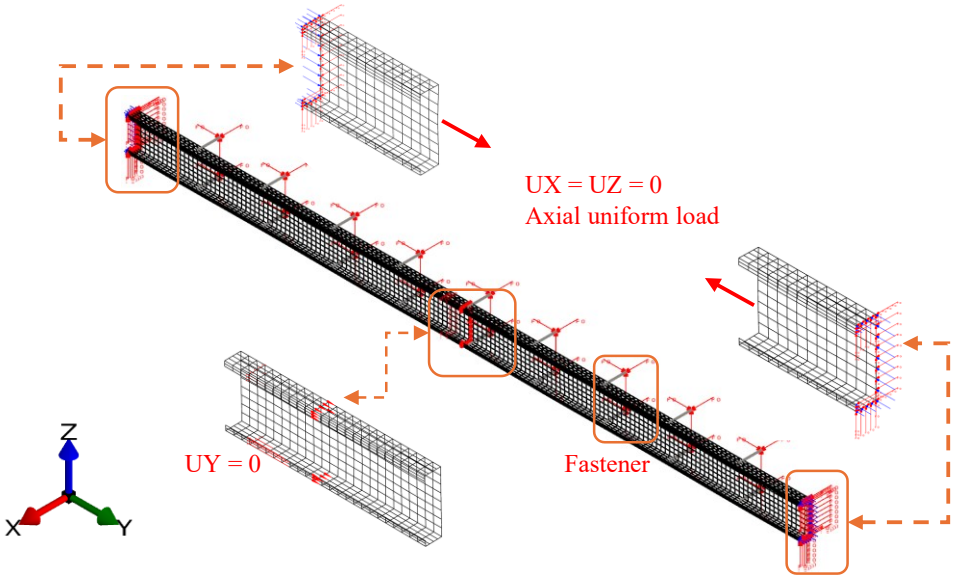

Figure 7: Loading and boundary conditions used in the shell finite element model

4.2. Parametric analysis

During the fire tests, the fire was allowed to grow, develop, and burn out naturally. The structure withstood the fire without collapse, as intended, since allowing structural collapse of the ten-story building on the shake table would not have been safe or practical. In this section, numerical modeling is used to examine (i) how different earthquake-induced damage to gypsum boards and fasteners would have affected the nonuniform temperature histories, critical temperatures, and buckling failure modes of Level 6 wall studs; and (ii) how the Level 6 wall studs would have responded under the test fire but with higher applied loads, to assess their safety margin during the fire test. The effect of earthquake damage was notably captured through assuming three levels of fastener restraint: (1) undamaged fasteners, assuming full stiffness; (2) partially damaged, assuming a 50% reduction in fastener stiffness; and (3) fully damaged, assuming no restraint from fasteners. Three gypsum thicknesses (5 mm, 10 mm, and 15.9 mm) were also considered to represent different levels of thermal protection that may result from gaps and integrity failure in the sheathing. This technique also allows indirectly evaluating the effect of different fire severity (i.e., while the thermal boundary conditions are consistently defined by the measured compartment temperatures, varying the gypsum board thickness in the model results in different temperature histories in the steel). Finally, five axial load levels were considered, equal to 1×, 2×, 4×, 8×, and 10× the load carried by the stud during the test, corresponding to load ratios (as a ratio of the ambient temperature capacity) of 0.075, 0.15, 0.30, 0.60, and 0.75, respectively.

Figure 8 presents the thermal results obtained assuming different gypsum thicknesses. Plotted are the compartment temperature, the hot-flange temperature, cold-flange temperature, and temperature difference between flanges. The results indicate that gypsum protection effectively reduces both the peak steel temperature and the heating rate. The peak compartment temperature reached 931 °C, whereas the peak hot-flange temperatures were 694 °C, 565 °C, and 401 °C for the three gypsum thicknesses considered, respectively. It is also clear that the rate of heating of the steel increases significantly with a reduction in gypsum thickness. Gypsum protection both reduced the steel peak temperature and delayed its occurrence.

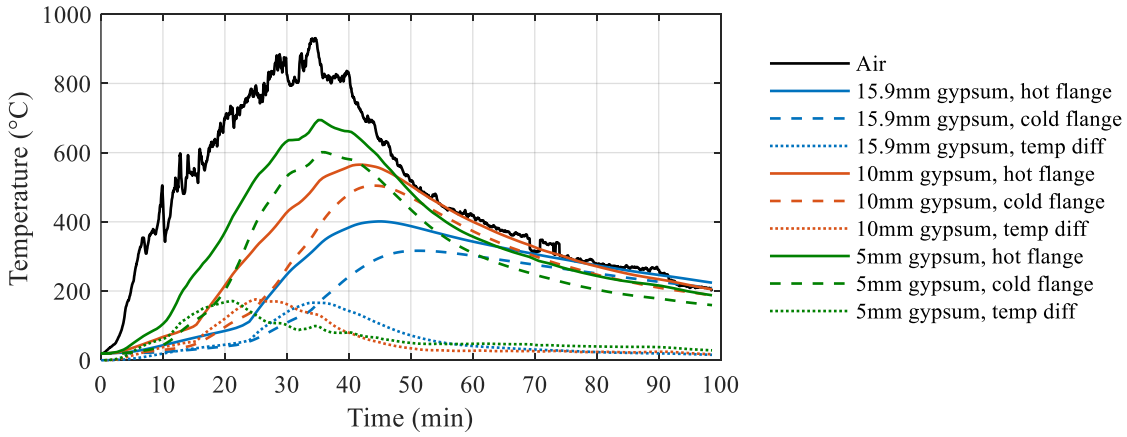

Figure 8: Temperature in the CFS stud obtained from models with different thickness of gypsum sheathing

Figure 9 shows the structural analysis results. Transient shell analyses were conducted under different applied loads and fastener assumptions, with the temperature histories in the shells obtained from thermal analyses with the L6 test fire and different gypsum thickness assumptions.

The FEM results are plotted in terms of relationship between the applied load on the CFS stud and the temperature of the hot flange at failure. Results from the Direct Strength Method (DSM) conducted before the test (Niu *et al.*, 2025) and used to support the test design show conservative agreement with the FEM. Results from light-gauge steel frame tests (Ariyanayagam and Mahendran, 2014), labeled EXP, also align, validating the numerical model. Finally, the load-temperature reached in the CFS10 test is also plotted, showing the significant safety margin. The critical temperature for the full fasteners configuration is slightly higher than that for the half fasteners configuration, and both are substantially higher than that for the no fasteners case. In addition, the critical temperature increases as the load ratio decreases.

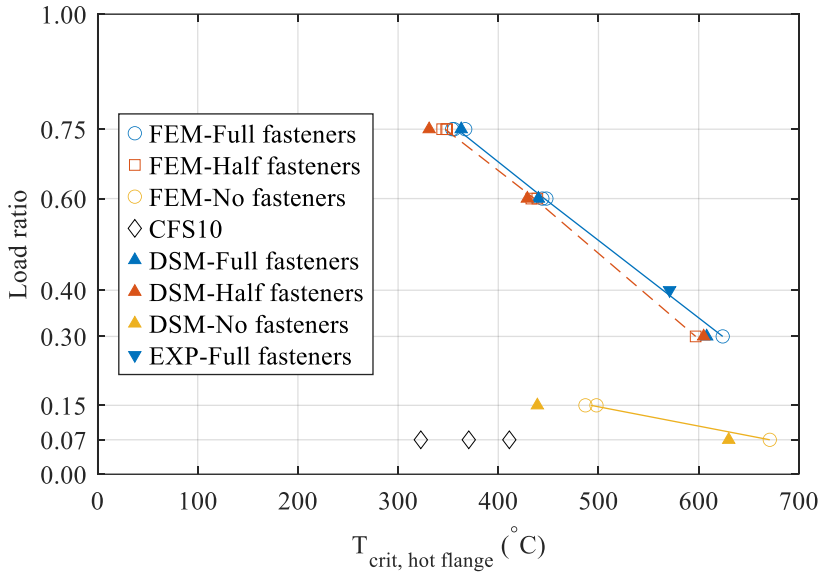

Figure 9: Parametric analysis results: critical hot-flange temperature versus load ratio for studs with and without fasteners. The load-temperature reached in the CFS10 test is also plotted, showing the significant safety margin.

The CFS wall members had a substantial safety margin during the CFS10 test. As seen in Figure 9, during the test, the maximum (average) steel temperature was about 410 °C, while the axial force in the stud was about 7.5% of its ambient temperature capacity. With intact fasteners, the members could sustain at least eight times the load applied in the CFS10 fire tests. Even if all fasteners were assumed to fail, the members could still resist at least twice the test-applied load. Indeed, the FE transient shell analysis conducted under a load ratio of 0.15 (i.e., twice the load present during the actual test) predicted a critical temperature of about 490 °C. A simple DSM analysis was also conducted and predicted a critical temperature of 439 °C under a load ratio of 0.15, again confirming that even without any restraint from the fasteners, the wall studs would have survived the applied thermal exposure.

The predicted failure mode depends primarily on whether fasteners are present. Figure 10a shows the deformed shape at failure (amplified 10 times) for the CFS channel member with and without fastener restraint. The member without fasteners fails by global buckling, while the member restrained by fasteners fails by combination of local and distortional buckling. Figure 10b classifies the failure mode for the different cases run, including various applied loads and gypsum thickness. It is observed that the failure mode does not noticeably depend on the temperature or the load ratio.

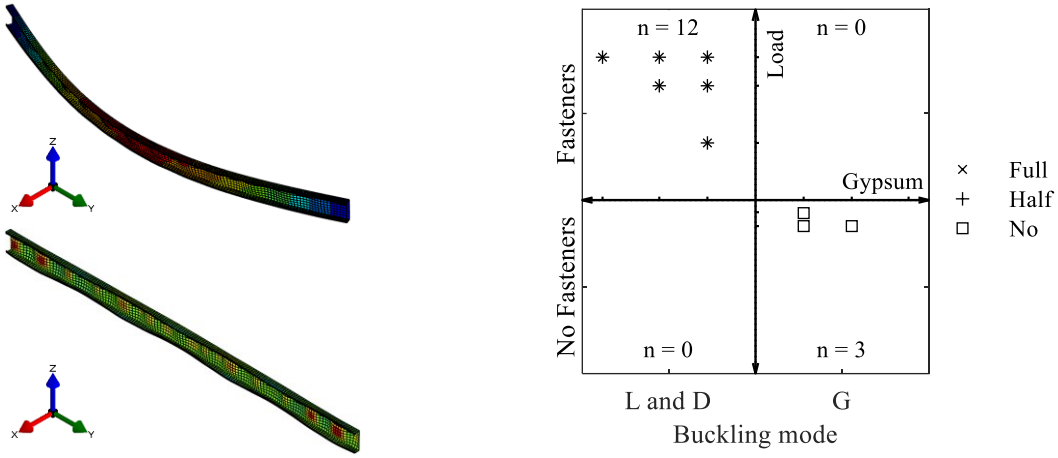

(a) (b)

Figure 10: Failure modes: (a) FE model deflected shape at failure with a scale factor of 10. (b) classification for studs with and without fasteners (local/distortional vs. global buckling)

The critical temperature is essentially insensitive to the heating rate, captured here through different gypsum-board thickness. Figure 11 illustrates the temperature fields of the wall stud at failure for a load ratio of 0.75 under different gypsum thicknesses. The cross-sectional nonuniform temperature distributions are similar across the cases, and the peak hot-flange temperatures are also comparable (354-367 °C). The time at which these failures occur would differ, because the steel member with the thinner gypsum sheathing heats up faster, but the temperature distribution leading to failure is very similar between the three configurations.

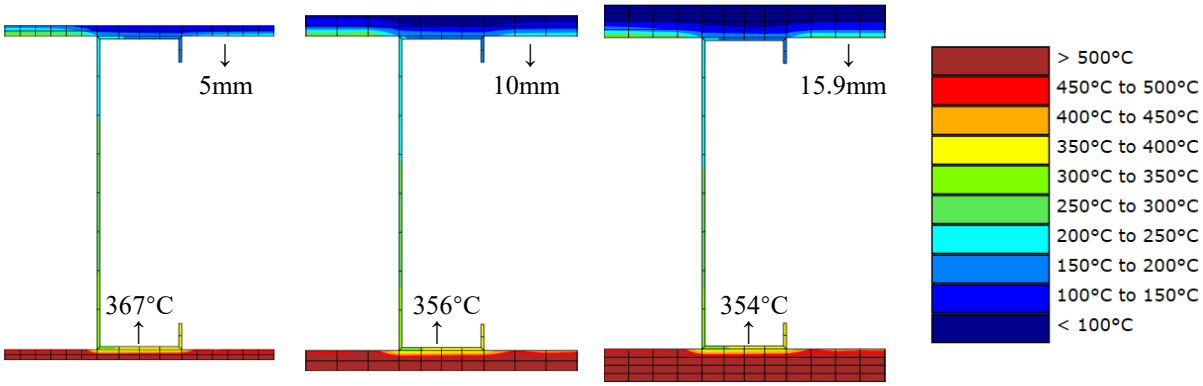

Figure 11: Temperature fields at failure for different gypsum board thicknesses (load ratio = 0.75)

5. Conclusions

This paper presented a numerical study of the fire response of cold-formed steel (CFS) wall assemblies. Full-scale post-seismic fire tests on a ten-story CFS building recently conducted at UCSD as part of the CFS-NHERI research project were used as benchmark for the numerical study. Thermal-structural finite element models, initially developed to inform the experimental program, were validated against the test data and used to further investigate the sensitivity of the CFS structural fire response. The main findings are summarized hereafter.

The FE thermal model, using the measured compartment temperatures as boundary conditions, provided accurate predictions of wall temperatures, including for the two flanges of the wall studs. The predicted studs flange temperatures fell within the envelope of the thermocouple measurements and were slightly higher than the measured average values. Both 2D and 3D FE thermal models were used to assess the influence of spatially non-uniform thermal boundary conditions on steel temperatures. The two approaches showed close agreement; the 3D analysis indicated that wall stud temperatures exhibited only minor spatial variability along the wall height.

The thermal-mechanical model was used to assess the stability of CFS wall studs under transient non-uniform temperature distributions obtained from the thermal analyses, accounting for temperature-dependent material properties and fastener restraint. The predicted critical temperatures were consistent with experimental data from the literature, while estimates using the simpler Direct Strength Method showed conservative agreement.

Parametric analyses were conducted for varying gypsum board thickness, fastener restraint conditions, and applied load levels. The results indicate that fastener restraint significantly increases the critical temperature of CFS members and directly governs the buckling failure mode. In addition, the critical temperature increases as the applied load ratio decreases. For the CFS10 building test, the wall studs still had significant reserve capacity, because their temperatures generally remained below 500 °C while the applied load was approximately 7.5% of their ambient temperature capacity; even assuming a complete loss of fastener restraint, the studs could still have sustained about twice the applied load.

Acknowledgement
This material is based upon work supported by the U.S. National Science Foundation (NSF) under award No. 2237623 "CAREER: Performance-Based Fire Design for Cold-Formed Steel Structures" (PI T. Gernay). The financial support is gratefully acknowledged.

References

A.D. Ariyanayagam, M. Mahendran. (2014). "Numerical modelling of load bearing light gauge steel frame wall systems exposed to realistic design fires", *Thin-Walled Structures*, 78 148–170.

ANSI/SDI AISI S100-2024: North American Specification for the Design of Cold-Formed Steel Structural Members, Washington, DC, USA, 2024.

ASCE/SEI 7-22: Minimum Design Loads and Associated Criteria for Buildings and Other Structures, *American Society of Civil Engineers*, Washington, DC, USA, 2022.

B.W. Schafer. (2008). "The direct strength method of cold-formed steel member design", *Journal of Constructional Steel Research*, 64 766–778.

C. Scawthorn, J.M. Eidinger, A. Schiff. (2005). "Fire following earthquake", ASCE Publications.

CEN, Eurocode 3: Design of Steel Structures - Part 1–2: General Rules - Structural Fire Design, 2005.

D. Bandula Heva, M. Mahendran. (2013). "Flexural-torsional buckling tests of cold-formed steel compression members at elevated temperatures", *Steel and Composite Structures*, 14 205–223.

E. Ali. (2021). "Influence of non-uniform elevated temperature on the structural stability and strength of gypsum-sheathed cold-formed steel beam channel members", *Journal of Civil Engineering and Architecture*, 15 285.

J.C.B. Abreu, L.C. Vieira Jr, T. Gernay, B.W. Schafer. (2021). "Cold-formed steel sheathing connections at elevated temperature", *Fire Safety Journal*, 123 103358.

J. Xie, T. Gernay. (2025). "Experimental study on the behavior of cold-formed steel lipped channels under uniform and non-uniform elevated temperatures", *Proceedings of the Structural Stability Research Council Annual*.

J.-M. Franssen, T. Gernay. (2017). "Modeling structures in fire with SAFIR®: Theoretical background and capabilities", *Journal of Structural Fire Engineering*, 8 300–323.

L.Y. Cooper. (1997). “The Thermal Response of Gypsum-panel/steel-stud Wall Systems Exposed to Fire Environments: A Simulation for Use in Zone-type Fire Models”, National Bureau of Standards.
M. Feng, Y.-C. Wang, J.M. Davies. (2003). “Thermal performance of cold-formed thin-walled steel panel systems in fire”, *Fire Safety Journal*, 38 365–394.
N.D. Kankanamge, M. Mahendran. (2011). “Mechanical properties of cold-formed steels at elevated temperatures”, *Thin-Walled Structures*, 49 26–44.
S. Torabian, Z.S. Nia, B.W. Schafer. (2016). “An archetype mid-rise building for novel complete cold-formed steel buildings”, Missouri University of Science and Technology.
S. Lee, R. Davidson, N. Ohnishi, C. Scawthorn (2008). “Fire following earthquake—Reviewing the state-of-the-art of modeling”, *Earthquake Spectra*, 24 933–967.
S. Gunalan. (2011). “Structural behaviour and design of cold-formed steel wall systems under fire conditions”, PhD Thesis, Queensland University of Technology.
S. Gunalan, Y.B. Heva, M. Mahendran. (2014). “Flexural–torsional buckling behaviour and design of cold-formed steel compression members at elevated temperatures”, *Engineering Structures*, 79 149–168.
S. Adany. (2006). “Buckling analysis of cold-formed steel members using CUFSM: conventional and constrained finite strip methods”, *CCFSS Proceedings of International Specialty Conference on Cold-Formed Steel Structures*(1971-2018).
T.C. Hutchinson, X. Wang, G. Hegemier, B. Meacham, P. Kamath, F. Sesma, K. Holcomb. (2017). “Earthquake and post-earthquake fire performance of a mid-rise cold-formed steel framed building”, *2017 SEAOC Convention*.
T.C. Hutchinson, X. Wang, G. Hegemier, P. Kamath, B. Meacham. (2021). “Earthquake and Postearthquake Fire Testing of a Midrise Cold-Formed Steel-Framed Building. I: Building Response and Physical Damage”, *Journal of Structural Engineering*, 147 04021125.
V.M. Zeinoddini, B.W. Schafer. (2012). “Simulation of geometric imperfections in cold-formed steel members using spectral representation approach”, *Thin-Walled Structures*, 60 105–117.
W. Chen, J. Ye, Q. Wang, J. Jiang. (2020). “Postearthquake fire experiments of cavity-insulated cold-formed steel load-bearing walls lined with plasterboards”, *Journal of Constructional Steel Research*, 167 105845.
X. Yan, Y. Xia, H.B. Blum, T. Gernay. (2020). “Elevated temperature material properties of advanced high strength steel alloys”, *Journal of Constructional Steel Research*, 174 106299.
Y. Niu, Z. Li, S. Enright, J. Dillard, T. Hutchinson, R. Emberley, B. Meacham, T. Gernay. (2025). “Numerical modeling of the post-earthquake fire performance of cold-formed steel members”, *Structural Stability Research Council*, Louisville, Kentucky.
Z. Li, B. Schafer. (2010). “Buckling analysis of cold-formed steel members with general boundary conditions using CUFSM conventional and constrained finite strip methods”, *CCFSS Proceedings of International Specialty Conference on Cold-Formed Steel Structures (1971 - 2018)*, Missouri University of Science and Technology.